Pergamon

Int. J. Solids Structures Vol. 32, No. 8/9, pp. 1121–1133, 1995

0020-7683/95 $9.50 + .00

0020-7683(94)00178-2

ELASTO-PLASTIC CONSTITUTIVE MODELLING OF GRANULAR ASSEMBLY

CHING-LUNG LIAO, TA-PENG CHANG and DONG-HWA YOUNG
Department of Construction Engineering, National Taiwan Institute of Technology, Taipei, Taiwan 106, Republic of China

(*Received* 24 *September* 1992; *in revised form* 9 *July* 1994)

Abstract—A triaxial elasto-plastic stress–strain relationship of a continuum solid derived from a base of granular assembly is presented. It shows a macroscopic material nonlinearity by considering the local geometric nonlinearity of the material on the microscopic level of the granular assembly. For a given strain increment causing both elastic and plastic strain increments in an assembly, the elastic strain is calculated by the known uniform strain theory of granular materials, and the corresponding plastic strain increment is computed from the mechanism resulting from the strain due to slip between particles. Responses of two construction materials, steel and concrete, predicted by the proposed constitutive law are illustrated. Some other well-known physical phenomena like dilatation, necking and the confinement effect are also addressed under various loading cases, including uniaxial tension and compression, cyclic loading, biaxial and triaxial loadings.

1. INTRODUCTION

The macroscopic nonlinearity of materials can be considered a result of local geometric nonlinearity at the microscopic level. However, any description of nonlinearity at the microscopic level is not meaningful without the accompanying micromechanical constitutive models of granular assembly. Also, the micromechanics of a granular material provides a means of interpreting the discrepancy in the predicted strengths for most engineering materials, between the value determined by considering their physical properties on a microscopic scale and that on a macroscopic scale. Consequently, the study of micromechanical behavior of granular materials has been an active research subject during the past 20 years. Some numerical analyses of granular materials, e.g. the well-known discrete element method (Cundall, 1971; Cundall and Strack, 1979, 1983), have been proved feasible for verifying theoretical results (Drescher and deJosselin deJong, 1972; Oda 1972; Shukla *et al.*, 1990). Generally, the micromechanic theories of granular materials are derived from the effects of the fabric property and the contact law between packing particles on the assembly behavior (Chang, 1987; Bathurst and Rothenburg, 1988; Chang and Misra, 1989, 1990; Chang and Ma, 1991), and various constitutive equations based on different hypotheses have been proposed to verify those theories. Among others, some researchers (Liao and Chang, 1989; Chang and Misra 1989, 1990) developed a microstructural continuum model based on a uniform strain assumption. On the other hand, local defects and stability of granular particles during the loading process have been proved to influence the response of granular material (Liao and Chang, 1990); formulation of micromechanical behavior of granular materials based on the concept of fabric tensor (Oda *et al.*, 1982) have been reported to yield satisfactory results (Cowin and Satake, 1978; Christoffersen *et al.*, 1981; Chang, 1987; Bathurst and Rothenburg, 1988; Satake and Jenkins, 1989); and a plasticity model based on granular mechanics for a range of regular packings of identical rigid spheres has been reported (Thornton and Barnes, 1982).

Concepts of the proposed constitutive equations presented in this paper are based on the mechanism of slip and separation between particles. The concept of slip has been used by Taylor (1938) to model the stress–strain relationship of face-centered cubic (f.c.c.) polycrystalline metals. There are 12 slip systems for f.c.c. crystals, of which only five slip systems are required to define the strain of aggregate produced by slips alone, while it is assumed that there is no volumetric change of strain. Taylor (1938) has applied the principle

of virtual work to determine which five out of the 12 slip systems are active. He also assumes a static constraint in the model, in which the strain in each grain is uniform and equal to the macroscopic aggregate strain. In this paper, instead of prescribing static constraints, as applied in the early slip models (Taylor, 1938; Batdorf and Budiansky, 1949; Lin and Ito, 1966), kinematic constraints similar to that of a microplane model (Bazant and Oh, 1985; Prat, 1987) are imposed on the granular assembly to derive the shear strain tensor of a particle. The slip plane is assumed to be dependent on the resolved shear stress alone and independent of the normal pressure on the plane. Both the effects of normal pressure and the resolved shear force on the interface of particles are included in the current formulation. In addition to the plastic deformation due to excessive slip, the degradation of stiffness of assembly due to particle separation is also considered. Furthermore, the slip systems of granular assembly in general may occur in an infinite number of ways, and it is the aim of this study to present an approach that is suitable to model various types of loading histories and different materials. Numerical examples of responses of two commonly used construction materials, steel and concrete, under various loading cases, e.g. uniaxial, biaxial, standard triaxial, cyclic loadings, are illustrated.

2. PLASTIC STRAINS OF GRANULAR ASSEMBLY

During the loading process, a granular assembly will experience both elastic and plastic deformations. The calculation of elastic strain increment for a packing of granular assembly is based on an affine assumption, that is, the particle displacement can be obtained by an assumed uniform strain field, while plastic strains result from local deformation of granular assembly. A slip between particles occurring at a microscopic level will contribute to its macroscopic deformation and can be considered as the cause of plastic strain. In this study, the plastic strain is assumed to be obtained by accumulating local plastic deformation individually without interference among particulates. Thus it belongs to a non-affine assumption. The elastic and plastic strains of a particle are computed according to the given shear resistance between particles. For the following derivation of micromechanics, the granular assembly is assumed to be composed of equal-size rigid spherical particles.

2.1. *Particle strain due to slip at contact*

When a shear force between two particles exceeds its shear resistance, slip at contact occurs. The shear resistance of particles, $S_{\max}$, can be represented as follows when two particles are in a state of squeezing, i.e.

$$S_{\max} = R_s + \mu N, \tag{1}$$

where N is the contact normal force; R_s is the shear resistance when N is zero and μ is the coefficient of internal shear friction at contacts. If the contact normal force tends to separate two particles, eqn (1) is applicable until the bond strength at contact is reached. By checking the maximum shear stress against the allowable shear capacity of eqn (1) at the contact point of particles, the amount of slip Δ_{ni} can be obtained by subtracting the elastic portion from the total incremental displacement between two particles using the following equation:

$$\Delta_{ni} = \bar{\varepsilon}_{ij}\mathbf{b}_{nj} - \frac{S_{\max}}{K_i}, \tag{2}$$

where Δ_{ni} is the contact slip along local ith direction tangential to the contact normal $\mathbf{n}$; K_i is the initial tangential contact spring constant between particles; $\bar{\varepsilon}_{ij}$ is the mean packing strain, and $\mathbf{b}_{nj}$ is the branch vector (vector connecting the centroid of two contacted

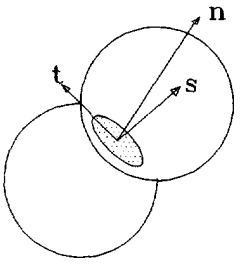

Fig. 1. Local coordinate system.

particles) along the **n** direction of the local coordinate system, as shown in Fig. 1. Note that the uniform strain theory (Chang and Misra, 1990) has been applied in eqn (1). If a slip occurs at a certain contact point between two particles, it is assumed that an equivalent local plastic shear strain is induced in both particles along the slip direction. This local plastic strain is related to the amount of shear deformations of the particles under consideration. As an example, a single typical particle a with slip increments Δ_{ns}^{ac} and Δ_{nt}^{ac} at contact point c along the **s** and **t** directions, respectively, on a tangential plane containing normal vector **n** is shown in Fig. 2. Then the total external complementary virtual work increment $\delta(\mathrm{d}W_{\mathrm{E}})$ due to a slip Δ_{ns}^{ac} and a virtual contact shear force δf_{ns}^{ac}, acting along the same **s** direction of the particle, is given by

$$\delta(\mathrm{d}W_{\mathrm{E}}) = -\Delta_{ns}^{ac}\,\delta f_{ns}^{ac} \quad \text{(no sum over } a, c, n \text{ and } s\text{)}. \tag{3}$$

The internal complementary virtual work of the particle, $\delta(\mathrm{d}W_{\mathrm{I}})$, due to a slip at c can be obtained by the volume integration over the product of strain increment and virtual stress of the particle, i.e.

$$\delta(\mathrm{d}W_{\mathrm{I}}) = \int_{V^a} \mathrm{d}\varepsilon_{ij}\,\delta\sigma_{ij}\,\mathrm{d}V, \tag{4}$$

where $\mathrm{d}\varepsilon_{ij}$ = incremental strain tensor of particle; $\delta\sigma_{ij}$ = virtual stress tensor; V^a = volume of particle; and i,j = 1–3. Note that the multiplication of the nine components of strain and stress in eqn (4) can be replaced by two single values $\mathrm{d}\varepsilon_{ns}$ and $\delta\sigma_{ns}$, which are the only two non-zero components when slip occurs, where $\mathrm{d}\varepsilon_{ns}$ and $\delta\sigma_{ns}$ are the strain increment and virtual stress in the **s** direction on the plane with a normal vector **n**, respectively. Thus eqn (4) becomes

$$\delta(\mathrm{d}W_{\mathrm{I}}) = \int_{V^a} \mathrm{d}\varepsilon_{ns}\delta\sigma_{ns}\,\mathrm{d}V = \mathrm{d}\varepsilon_{ns}^{*}\delta\sigma_{ns}^{*}V^a \quad \text{(no sum on } n \text{ and } s\text{)}, \tag{5}$$

where $\delta\sigma_{ns}^{*}$ and $\mathrm{d}\varepsilon_{ns}^{*}$ are the conjugate stress and strain of the particle, respectively. Although the values of $\delta\sigma_{ns}^{*}$ and $\mathrm{d}\varepsilon_{ns}^{*}$ can be selected arbitrarily, provided that they satisfy eqn (5), one of the two quantities may be defined first with certain physical significance and the

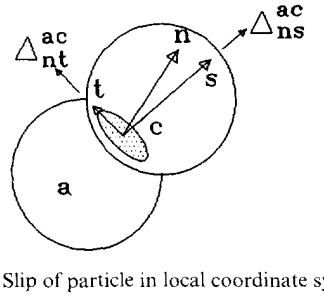

Fig. 2. Slip of particle in local coordinate system.

other may then be computed accordingly. If we assume that the stress and strain fields are nearly uniform for a particle subjected to boundary contact forces, we can select $d\varepsilon_{ns}^{*}$ as the mean value of $d\varepsilon_{ns}$ and $\delta\sigma_{ns}^{*}$ as the mean value of $\delta\sigma_{ns}$ of the particle, respectively. This assumption is simply an approximation to the calculation of virtual work of eqn (5). The deviation to the actual value depends on the boundary conditions of each particle in the assembly. Thus, according to the theorem of stress means (Landau and Lipschitz, 1959; Christoffersen *et al.*, 1981), the mean shear stress, $\bar{\sigma}_{ns}^{ac}$, of the particle a due to a contact shear force f_{ns}^{ac} at c is

$$\bar{\sigma}_{ns}^{ac} = \frac{1}{V^{a}} r_{n}^{ac} f_{ns}^{ac} \quad \text{(no sum over } a, c \text{ and } n\text{)}, \tag{6}$$

where r_{n}^{ac} is the component in the **n** direction of the position vector from the centroid of particle a to the contact point c. The average stress tensor introduced in eqn (6) has all the properties of Cauchy stress tensor in continuum mechanics (Rothenberg and Selvadurai, 1981; Chang and Misra, 1989). It satisfies the equation of static equilibrium and the relation between the traction and the internal stress. Substituting eqn (6) into eqn (5) gives

$$\delta(dW_{1}) = d\bar{\varepsilon}_{ns}^{ac}\delta\bar{\sigma}_{ns}^{ac}V^{a} = d\bar{\varepsilon}_{ns}^{ac}r_{n}^{ac}\delta f_{ns}^{ac} \quad \text{(no sum over } a, c, n \text{ and } s\text{)}, \tag{7}$$

where $d\varepsilon_{ns}^{*}$ in eqn (5) has been replaced by the mean strain increment, $d\bar{\varepsilon}_{ns}^{ac}$. By the principle of virtual work, the sum of virtual work resulting from internal forces and that from external forces for a solid in a state of equilibrium is zero, i.e.

$$\delta(dW_{1}) + \delta(dW_{E}) = 0. \tag{8}$$

From eqns (3) and (7), we can obtain the incremental mean strain $d\bar{\varepsilon}_{ns}^{ac}$ given as

$$\because \quad d\bar{\varepsilon}_{ns}^{ac}r_{n}^{ac}\delta f_{ns}^{ac} - \Delta_{ns}^{ac}\delta f_{ns}^{ac} = 0 \quad \text{(no sum over } a, c, n \text{ and } s\text{)}, \tag{9}$$

$$\therefore \quad d\bar{\varepsilon}_{ns}^{ac} = \frac{\Delta_{ns}^{ac}}{r_{n}^{ac}} \quad \text{(no sum over } a, c \text{ and } n\text{)}.$$

From eqn (9), therefore, it can be seen that the local strain of a particle due to slip is defined as the relative displacement Δ_{ns}^{ac} at contact, divided by r_{n}^{ac}, the arm measured from the center of the particle to the slip. Similarly, the local shear strain increment $d\bar{\varepsilon}_{nt}^{ac}$ along the orthogonal tangent direction **t** due to a slip Δ_{nt}^{ac} acting in the same direction is given by

$$d\bar{\varepsilon}_{nt}^{ac} = \frac{\Delta_{nt}^{ac}}{r_{n}^{ac}} \quad \text{(no sum over } a, c \text{ and } n\text{)}. \tag{10}$$

Because it is assumed that the local plastic deformations occur individually, the effects of $d\bar{\varepsilon}_{ns}^{ac}$ and $d\bar{\varepsilon}_{nt}^{ac}$ need to be transformed separately to the global coordinate system, and then combined. Therefore, the corresponding mean plastic strain increment tensor, $d\bar{\varepsilon}_{ij}^{ac}$, of a typical particle a in the global coordinate system due to a single slip at the contact point c, can be expressed in terms of $d\bar{\varepsilon}_{ns}^{ac}$ and $d\bar{\varepsilon}_{nt}^{ac}$ as follows:

$$d\bar{\varepsilon}_{ij}^{ac} = n_{i}s_{j}\, d\bar{\varepsilon}_{ns}^{ac} + n_{i}t_{j}\, d\bar{\varepsilon}_{nt}^{ac}. \tag{11}$$

Therefore, the incremental mean strain tensor of the particle, $d\bar{\varepsilon}_{ij}^{a}$, under a slip deformation is calculated by the summation of all individual strains distributed over all contact points, i.e.

$$\mathrm{d}\bar{\varepsilon}_{ij}^{a} = \sum_{c} d\bar{\varepsilon}_{ij}^{ac}. \tag{12}$$

2.2. *Equivalent plastic strain of packing*

In this paper, the equivalent mean plastic strain increment tensor of the packing, $\mathrm{d}\bar{\varepsilon}_{ij}^{\mathrm{p}}$, is collected from the value of each particular mean strain increment $\mathrm{d}\bar{\varepsilon}_{ij}^{a}$ of packing by a volume average, and is given by

$$\mathrm{d}\bar{\varepsilon}_{ij}^{\mathrm{p}} = \frac{1}{V}\sum_{a} \mathrm{d}\bar{\varepsilon}_{ij}^{a} V^{a}, \tag{13}$$

where the summation is carried over all the particles. Substituting eqns (11) and (12) into eqn (13) gives

$$\mathrm{d}\bar{\varepsilon}_{ij}^{\mathrm{p}} = \frac{1}{V}\sum_{a}\sum_{c} [n_i s_j \,\mathrm{d}\bar{\varepsilon}_{ns}^{ac} + n_i t_j \,\mathrm{d}\bar{\varepsilon}_{nt}^{ac}] V^{a}, \tag{14}$$

where the superscript p stands for plastic strain; the inner summation sums over all contact points c for the particle a, and the outer summation over all particles a of the packing; V^{a} is the volume of the particle; and V is the volume of the representative packing including voids. It can be shown that the volumetric change is equal to zero in eqn (14), i.e. $\mathrm{d}\bar{\varepsilon}_{ii}^{\mathrm{p}} = 0$.

Since the slip of particles can be regarded as an energy dissipation of the system, it follows that the plastic portion in eqn (14) is irreversible unless it is compensated by an equal but opposite permanent plastic strain imposed by a reverse loading. This idea may be easily extended to modeling a cyclic loading case, as will be shown later.

3. CONSTITUTIVE EQUATIONS

A general elasto-plastic stress–strain relationship based on the characteristics of granular materials is presented here. Time effect is not included in the formulation, therefore only elastic deformation and plastic deformation will be considered. Generally, upon loading, separation and/or slip between particles of granular assembly will occur. It is considered that slip is a relative contact motion produced by sliding and/or rolling of particles, such that the contact points always remain in contact after slip. Thus the deformed packing is only slightly rearranged to dissipate energy, but undertakes a permanent deformation. In this paper, since the global plastic deformation due to slips at all contact points is irreversible, it is assumed that the stabilized packing after slip deformation still behaves as an elastic solid. This phenomenon may be referred to as a "dissipative system". Further, slip motion is assumed to be the only cause of plastic strain. Since the permanent plastic strain increment resulting from this plastic response is subtracted from the total strain increment given by the unifrom strain theory (Chang and Misra, 1990), the corresponding stress increment associated with the remaining elastic strain increment can be obtained through generalized Hooke's law.

For a packing of granular assembly subjected to a slip deformation under combined stresses, the resulting strain of the packing is assumed to be decoupled into elastic and plastic components. Therefore, for a given external strain increment $\mathrm{d}\varepsilon_{kl}$ of the packing, the associated mean stress increment of packing is assumed to be equal to the elastic stress increment as given by

$$\mathrm{d}\bar{\boldsymbol{\sigma}}_{ij} = \mathbf{C}_{ijkl}(\mathrm{d}\varepsilon_{kl} - \mathbf{d}\bar{\boldsymbol{\varepsilon}}_{kl}^{\mathrm{p}}), \tag{15}$$

where $\mathbf{C}_{ijkl}$ is the fourth-order tensor of elastic moduli of the packing; $\mathrm{d}\bar{\boldsymbol{\sigma}}_{ij}$ is the incremental mean stress tensor; and $\mathrm{d}\bar{\boldsymbol{\varepsilon}}_{kl}^{\mathrm{p}}$ is the incremental plastic mean strain tensor. The tensor $\mathbf{C}_{ijkl}$ of elastic moduli can be calculated by the uniform strain theory (Chang and Misra, 1990),

based on the individual mechanical constants at each contact of the granular assembly, and is written as

$$\mathbf{C}_{ijkl} = \sum_{c} \mathbf{L}_i K_{jl} \mathbf{L}_k,$$

$$K_{jl} = n_j n_l K_n + s_j s_l K_s + t_j t_l K_t, \tag{16}$$

where $\mathbf{L}_i$ and $\mathbf{L}_k$ are branch vectors joining the centers of two particles; and K_n, K_s and K_t are stiffness constants between particles of the granular assembly in the directions of the local coordinate system **n**, **s** and **t**, respectively, as shown in Fig. 1, in which c denotes the location of contact point. In eqn (16), the letter c underneath the summation symbol indicates that the summation is carried over all contact points under consideration. The local coordinate system is constructed for each contact point by three orthogonal base unit vectors with the vector **n** normal to the contact area, and the tangent vectors **s** and **t** being chosen arbitrarily.

4. NUMERICAL EXAMPLES

For the following numerical formulations, all particles are assumed to be spheres of equal size, and major variables are the normal spring constant K_n, tangential spring constants K_s, K_t, shear resistance coefficients R_s (cohesion), μ (friction coefficient) and bond strength T (tensile strength) at contact between particles. The values of K_n, K_s and K_t can be expressed in terms of the initial Young's modulus and Poisson's ratio as given in the following equations (Chen, 1993):

$$K_n = C_m \frac{E}{(1-2v)},$$

$$K_s = K_t = C_m \frac{E(1-4v)}{(1+v)(1-2v)},$$

$$C_m = \frac{3V}{4N_c r^2}, \tag{17}$$

where N_c = total number of contacts of the whole packing; r = radius of particle; V = volume of packing including voids; E and v = Young's modulus and Poisson's ratio, respectively, of the packing in a representative volume. The parameters in eqn (17) are those factors that are required to characterize each different packing configuration. They must be properly estimated in order to comply with given material constants, i.e. Young's modulus E and Poisson's ratio v. In this paper, the effects of particle rotation are neglected and only the stretch spring and shear spring between particles are considered. The elastic limit of bonding strength determines whether the particles are still contacted under loading.

The response of each incremental loading follows eqn (15). At the very beginning, the material constants of the constitutive law are calculated by assuming the packing is in an elastic state, and are then used to calculate the strain of the packing under the given loading. From this strain increment field the corresponding displacement increment field can be obtained by the assumed affine displacement field for elastic strain and non-affine displacement field for plastic strain, as previously discussed. When the bond between particles fails under an applied load, the local normal stiffness K_n drops to zero at the contact points, and the elasticity matrix $\mathbf{C}_{ijkl}$ in eqn (15) is reformed. By checking the displacement at each contact against the allowable elastic limit, the amount of slip of the particles can be found. Finally, from eqns (12) and (14), the average plastic strain of the packing is obtained and then substituted into eqn (15) to calculate the stresses or strains. The same procedure is repeated until the end of load process is reached. The flow chart for this numerical procedure

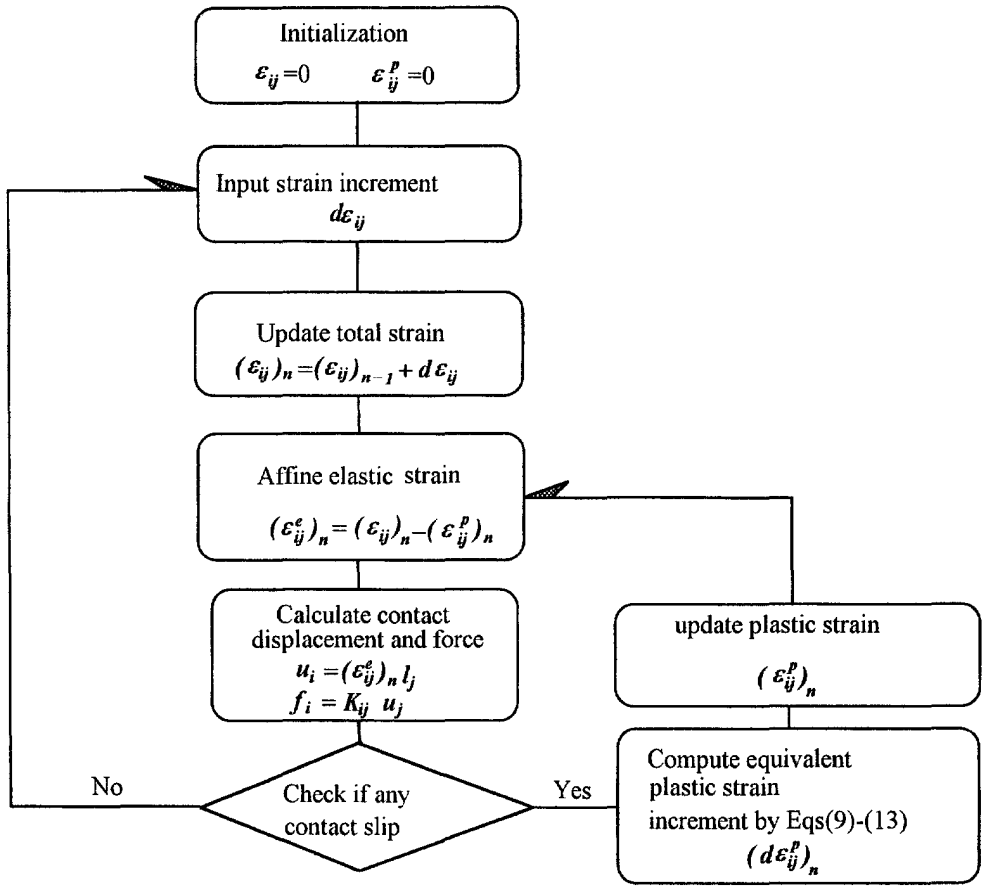

Fig. 3. Flow chart for numerical calculations.

is given in Fig. 3. Detailed numerical data will be given in the following individual illustration. Responses of two commonly used construction materials, i.e. concrete and steel, under several loading conditions, will be illustrated in this paper to demonstrate the applications of the proposed elastic-plastic constitutive model of granular materials.

4.1. *Response of steel with different strengths*

Because the Young's moduli E and Poisson's ratio v of various structural steels are insensitive to their compositions, E and v are assumed to be 207 GPa and 0.24, respectively, in the following examples. The strength of steel depends on its slip resistance, or shear resistance upon the dislocation motion, which is a function of particle size, coordination number and contact mechanical properties. This shear resistance is assumed to be provided by cohesion only. A key concept to properly simulate the response of steel using the current model is that the ratio of normal strength to shear resistance at contacts between particles should be large enough to assure that the slip will occur before separation or crushing of the particles. The resulting tensile and compressive stress–strain curves are shown in Fig. 4, which resembles the behavior of an elastic-perfectly-plastic material. It can be seen from the response curves that the volumetric ratio increases with strain up to the yield point and remains constant thereafter, which means that, in order to maintain a constant volume with an increasing longitudinal strain during the loading process, the lateral strain must decrease. Thus a necking phenomenon of steel is implied in this numerical simulation, which is consistent with the observed behavior of steel in real life.

The results of a cyclic load test for three elastic-perfectly-plastic steels are given in Fig. 5. The plastic strain introduced in one direction will not be recovered in the unloading phase until yielding occurs again under a reverse loading and produces an equal but opposite plastic strain. The residual stresses during the reverse of loading that may cause

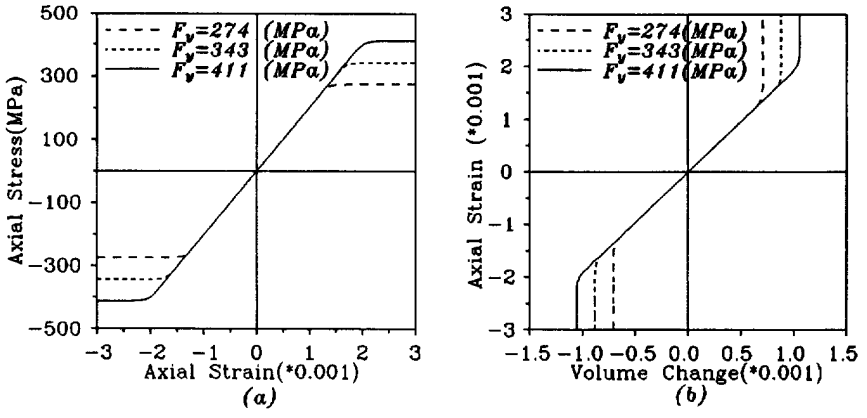

Fig. 4. Response curves for various steels: $F_y = 274$ (MPa), $F_y = 343$ (MPa), $F_y = 411$ (MPa), $F_y = 274$ (MPa), $F_y = 343$ (MPa), $F_y = 411$ (MPa).

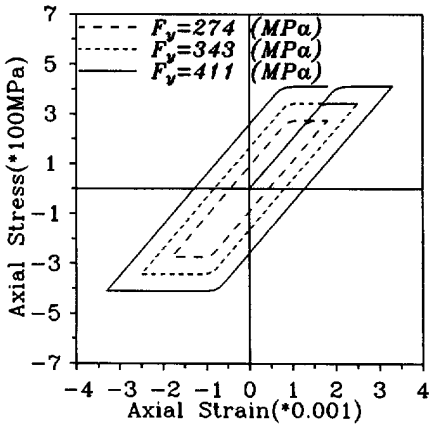

Fig. 5. Stress–strain curves of cyclic loadings: $F_y = 274$ (MPa), $F_y = 343$ (MPa), $F_y = 411$ (MPa).

Bauchinger's effects are not considered for the moment. Thus in Fig. 5 the behavior in compression is almost the same as that in tension.

4.2. *Response of concrete under uniaxial loading*

In the subsequent numerical examples of concrete, the initial Poisson's ratio is selected as 0.20 and the initial Young's modulus E_c corresponding to a given 28-day compressive strength f'_c is obtained through the following empirical formula (Mindess and Young, 1981), eqn (18), in order to comply with most testing conditions for normal weight concretes,

$$E_c = 4.730\sqrt{f'_c}\ \text{GPa}. \tag{18}$$

For most cementitious materials, such as concrete, the bond cracks and micro-cracks due to shrinkage exist even before the loading is applied. These cracks are relatively stable until the concrete experiences a stress of about 30% of its ultimate strength, and thereafter they begin to propagate. At a stress of about 70–90% of the ultimate strength, mortar cracks start to appear and merge with the existing bond cracks and micro-cracks to form continuous cracks. Beyond the critical stress point, i.e. the point at which the concrete volume begins to dilate or Poisson's ratio begins to increase, these continuous cracks then grow rapidly at the stress near the concrete failure strength until failure.

In general, aggregate strength is always large enough to prevent crushing, except in high-strength concretes or light-weight concretes, where mortar exhibits a relatively higher strength. The strength of the loading chain through aggregates and mortars in compression is much higher than that in tension. Thus, even when concrete is subjected to an external

Table 1. Results of concrete with various strengths

Material properties				
E_c(GPa)	ν	f'_c (MPa)	ε_c	f_t (MPa)
21	0.20	21.00	0.00105	3.86
25	0.20	28.00	0.00120	5.15
28	0.20	35.00	0.00130	6.23
31	0.20	42.00	0.00140	7.90

compressive loading other than a hydrostatic load, the failure is still controlled by its tensile capacity, i.e. its crack resistance. Therefore, the strength of concrete depends on the bond strength between particles, i.e. the strength of mortar matrix, which is a function of cement property, particle size and contact surface condition. The key idea to predict correct strength using the proposed model is using an appropriate value of bond capacity between particles. This value also determines the tensile strength of concrete.

The uniaxial responses of concretes obtained from the proposed constitutive law are shown in Table 1. The tensile strengths of concretes are also calculated in the table, which range from $0.1f'_c$ to $0.2f'_c$, approximately. These results are reasonable as compared with the real tensile strengths of concrete (Mindess and Young, 1981).

The corresponding stress–strain behaviors of these concretes are shown in Fig. 6. From Fig. 6(b), it can be seen that the volumetric strain decreases with compressive loading until the concrete is about to reach its ultimate strength, and then the concrete starts to dilate and shows a rapid increase of dilatancy near its peak strength. This behavior is consistent with previous experimental results (Kupfer *et al.*, 1969). Meanwhile, through numerical manipulation, it is observed that the value of shear friction affects only the portion of the stress–strain curves beyond peak strength.

In the above examples, the ultimate strains at peak stresses are slightly lower than previous reported values, which range from 0.0015 to 0.002 (Kupfer *et al.*, 1969). This discrepancy can be attributed to the fact that an idealized simple assumption in the microscopic constitutive law is applied to a rather heterogeneous concrete material in contrast to the previous homogeneous material of steel. For instance, a single value of bond strength is applied to the concrete packing for both curves in the Fig. 6. This assumption neglects the fact that various bond strengths are randomly distributed over the material due to the inherent properties of concrete in practice. If this factor had been considered in the simulation, the stress–strain curve would have softened gradually and the ultimate strain at peak stress would have been slightly higher, depending upon the degree of scattering. As a matter of fact, this assertion had been partially confirmed in several numerical trials. In Fig. 6(b), the compaction of concrete occurs up to the peak stress, and thereafter exhibits a pattern of dilatancy. This behavior has been verified by experiment (Kupfer *et al.*, 1969). For

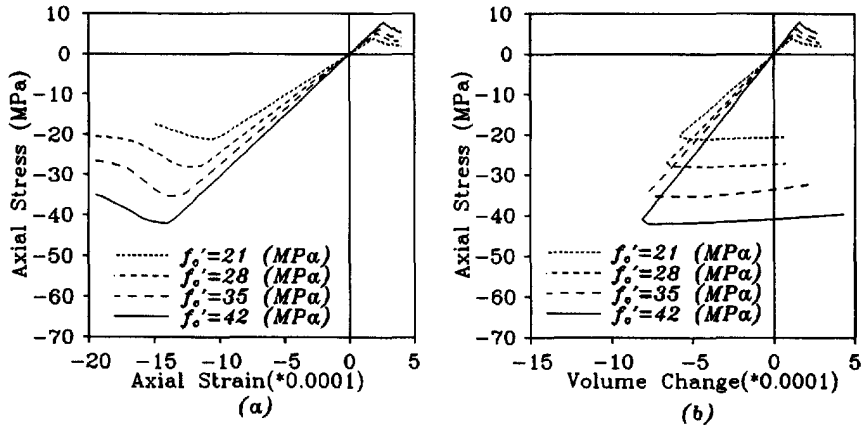

Fig. 6. Response curves for various concretes: $f'_c = 21$ (MPa), $f'_c = 28$ (MPa), $f'_c = 35$ (MPa), $f'_c = 42$ (MPa), $f'_c = 21$ (MPa), $f'_c = 28$ (MPa), $f'_c = 35$ (MPa), $f'_c = 42$ (MPa).

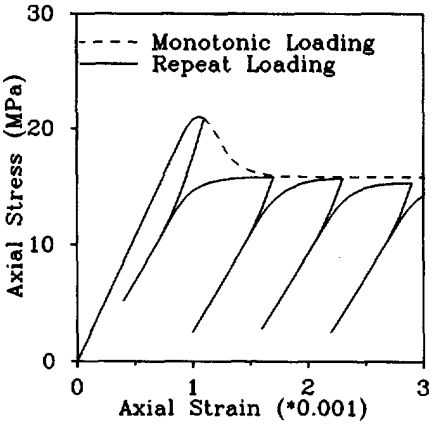

Fig. 7. Concrete response under cyclic loading. Monotonic loading; Cyclic loading.

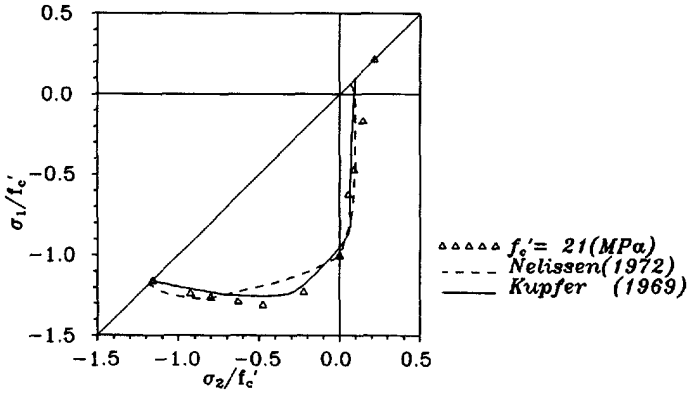

Fig. 8. Concrete under biaxial loading: $f_c' = 21$ (MPa), Nelissen (1972), Kupfer *et al.* (1969).

concretes under cyclic loading, the results are illustrated in Fig. 7, together with the results from monotonic loading.

4.3. *Response of concrete under biaxial loading*

The response of concrete under biaxial loading is of great importance, because in many circumstances concrete members need to be analyzed in a biaxial state. Test data (Kupfer *et al.*, 1969; Nelissen, 1972) have indicated that the maximum strength increase is approximately 25% at a stress ratio of $\sigma_1/\sigma_2 = 0.5$, and is about 16% at an equal biaxial compression state ($\sigma_1/\sigma_2 = 1.0$). These strength increases are also dependent on the compressive strength of concrete.

The proposed model is also applied to a concrete test under biaxial loadings, as shown in Fig. 8. In Fig. 8, the numerical values show a satisfactory match with the experimental data. It should pointed out that all the contact properties used in this example are the same as those obtained from previous uniaxial examples. All the numerical values are compared in Table 2.

Table 2. Results of concrete under various biaxial loadings

$f_c' = 21$ (MPa)		Kupfer *et al.* (1969) ($f_c' = 19.1$ MPa)		Nelissen (1972)	
σ_1/f_c'	σ_2/f_c'	σ_1/f_c'	σ_2/f_c'	σ_1/f_c'	σ_2/f_c'
0.219	0.219	0.100	0.100	0.064	0.064
−1.000	0.000	0.024	0.092	−1.000	0.000
−1.227	−0.222	−1.230	−0.290	−1.100	−0.182
−1.260	−0.800	−1.250	−0.660	−1.273	−0.836
−1.158	−1.158	−1.160	−1.160	−1.182	−1.182

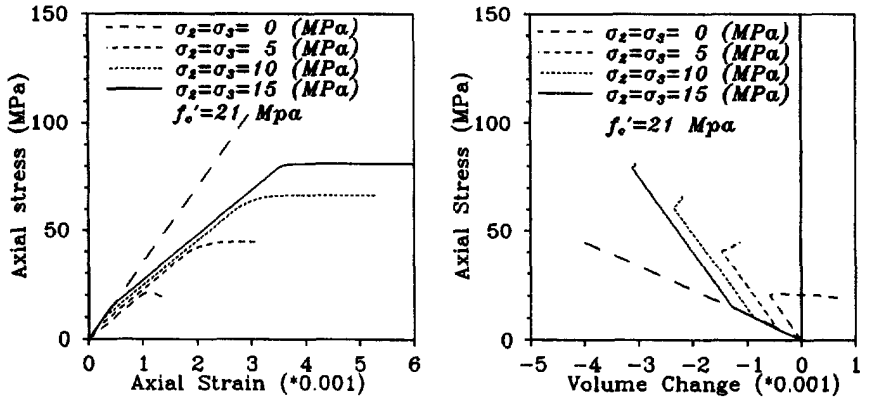

Fig. 9. Concrete response under various confinements: $\sigma_2 = \sigma_3 = 0$ (MPa), $\sigma_2 = \sigma_3 = 5$ (MPa), $\sigma_2 = \sigma_3 = 10$ (MPa), $\sigma_2 = \sigma_3 = 15$ (MPa), $f'_c = 21$ (MPa), $\sigma_2 = \sigma_3 = 0$ (MPa), $\sigma_2 = \sigma_3 = 5$ (MPa), $\sigma_2 = \sigma_3 = 10$ (MPa), $\sigma_2 = \sigma_3 = 15$ (MPa), $f'_c = 21$ (MPa).

4.4. *Response of concrete with different degrees of confinement*

Confinement effects of concrete are important in the design of reinforced concrete structures, especially when considering the failure mode of concrete changing from brittle to ductile. In practice, concrete is usually confined by transverse reinforcement in the form of closely spaced steel spirals or hoops. The increase of lateral pressure can substantially increase the ultimate strength and ductility of concrete. Lateral confinement also reduces the tendency of internal cracking and unstable volume increase just prior to failure.

When using the proposed model, concrete is under a hydrostatic confinement first, and then a uniaxial increase of strain is applied incrementally up to the point of failure. The resulting stress–strain curves for concrete with strengths, $f'_c = 21$, 35 and 42 MPa, respectively, under standard triaxial loading are illustrated in Fig. 9. The dilatancy of concrete is also shown in Fig. 9(b). The gain of strength and ductility as a result of confinement effects is listed in Table 3.

Previous results of concrete experiments with confinement effect have shown that the strength increase is approximately 4.1 times the lateral pressure (Richart *et al.*, 1928). In the current study, axial strength increases about four times the confining pressure as the confined pressure reaches its peak value. The results show a good agreement of confined concrete strengths between numerical and experimental data. However, the ultimate strains at peak stress in the example are lower than previously reported values (between 0.0021 and 0.0050) (Ahmad and Shah, 1982). The reason for this discrepancy is similar to that mentioned in the discussion for uniaxial load, i.e. the proposed model assumes an idealized contact property neglecting the inherent randomly distributed heterogeneous properties of concrete.

Table 3. Results of concretes with various confinement pressures

Confined pressure	Concrete testing									Richart *et al.* (1928)	
	$f'_c = 21$ (MPa)			$f'_c = 35$ (MPa)			$f'_c = 42$ (MPa)				
$\sigma_2 = \sigma_3$	ε_1	σ_1	C_0	ε_1	σ_1	C_0	ε_1	σ_1	C_0	σ_1	C_0
0.0	0.0011	21.95		0.0013	35.00		0.0014	42.00		20.42	
5.0	0.0020	41.13	4.04	0.0020	55.58	4.00	0.0020	62.59	4.02	40.51	4.05
10.0	0.0029	61.88	4.09	0.0026	75.87	4.04	0.0026	83.08	4.02	60.59	4.02
15.0	0.0042	83.04	4.13	0.0032	96.51	4.02	0.0032	103.57	4.02	80.68	4.02

Note: $C_0 = (\sigma_1 - f'_c)/\sigma_2$.

5. DISCUSSION AND CONCLUSION

From the theoretical derivations and numerical results of this study, the following conclusions are drawn:

(1) The proposed constitutive model is based on the idea of slip of particles in a granular assembly, which is a discrete approach. This model, however, can be satisfactorily applied to predicting the response of continuum media, such as steel and concrete under various loading cases. Taking concrete as an example, using a unique contact property, the model offers a satisfactory match with experimental data in four different loading histories: uniaxial, biaxial, triaxial and cyclic. Thus it can be anticipated that the proposed model is also applicable to a general multi-axial loading condition, e.g. all three principal stresses are independently applied.

(2) The proposed model provides a proper description of the dilatancy of concrete at a stress level near the failure strength, which is quite useful in the design of steel confinement for reinforced concrete members.

(3) Various phenomena of materials, including necking of steel, cyclic loading response, volume change from contraction to expansion, strain-softening beyond the peak strength and elastic-perfectly-plastic response can also be properly represented by the current approach. Therefore, the proposed constitutive model provides a wide range of application to simulating the response of other materials with complex properties.

Acknowledgement—The authors gratefully acknowledge the financial support provided by the National Science Council of the Republic of China, through the grants NSC81-0410-4011-10, NSC81-0410-E011-13 and NSC82-0410-E011-086 to the National Taiwan Institute of Technology, for the work presented in this paper. The valuable comments on this work by Professor Ching S. Chang of the University of Massachusetts are also greatly appreciated.

REFERENCES

Ahmad, S. H. and Shah, S. P. (1982). Stress–strain curves of concrete confined by spiral reinforcement. *ACI J.* **79–49,** 484–490.

Batdorf S. and Budiansky, B. (1949). A mathematical theory of plasticity based on the concept of slip. National Advisory Committee for Aeronautics, Technical Note No. 1871.

Bathurst, R. J. and Rothenburg, L. (1988). Micromechanical aspects of isotropic granular assemblies with linear contact interactions. *J. Appl. Mech.* **55**(1), 17–23.

Bazant, Z. P. and Oh, B. H. (1985). Microplane model for progressive fracture of concrete and rock. *J. EM ASCE* **111,** 559–582.

Chang, C. S. (1987). Micromechanical modelling of constitutive relations for granular material. In *Micromechanics of Granular Materials* (Edited by M. Satake and J. T. Jenkins), pp. 271–278. Elsevier, Amsterdam.

Chang, C. S. and Ma, L. (1991). A micromechanical-based micropolar theory for deformation of granular solids. *Int. J. Solids Struct.* **28**(1), 67–86.

Chang, C. S. and Misra, A. (1989). Computer simulation and modelling of mechanical properties of particulates. *Comput. Geotech.* **7**(4), 269–287.

Chang, C. S. and Misra, A. (1990). Application of uniform strain theory to heterogeneous granular solids. *J. Engng Mech. ASCE* **116**(10), 2310–2328.

Chen, B. H. (1993). Nonlinear constitutive law for granular materials. Masters Thesis, National Taiwan Institute of Technology, Taipei, Taiwan.

Christoffersen, J., Mehrabadi, M. M. and Nemat-Nasser, S. (1981). A micro-mechanical description of granular material behavior. *J. Appl. Mech.* **48**(2), 339–344.

Cowin, S. C. and Satake, M. (1978). Continuum mechanical and statistical approaches in the mechanics of granular materials. *Gakujutsu Bunken Fukyukai.* Tokyo, Japan.

Cundall, P. A. (1971) A computer model for simulating progressive, large-scale movements in block rock systems. *Proc. Symp. Int. Soc. rock Mechanics,* Nancy II, No. 7.

Cundall, P. A. and Strack, O. D. L. (1979). A discrete numerical model for granular assemblies. *Geotechnique* **29,** 47–65.

Cundall, P. A. and Strack, O. D. L. (1983). Model of microscopic mechanics in granular material. In *Mechanics of Granular Materials, New Models and Constitutive Relations* (Edited by J. T. Jenkins and M. Stake).

Drescher, A. and deJosselin deJong, G. (1972). Photoelastic verification of a mechanical model for the flow of a granular material. *J. Mech. Phys. Solids* **20**(2), 337–351.

Kupfer, H., Hilsdorf, H. K. and Rusch, H. (1969). Behavior of Concrete under Biaxial Stresses. *J. ACI,* **66,** 656–666.

Landau, L. D. and Liphschitz, E. M. (1959). *Theory of Elasticity.* Pergamon Press, Oxford.

Liao, Ching L. and Chang, Chang S. (1992) A microstructural finite element model for granular solids. *Engng Comput.* **9,** 267–276.

Lin, T. H. and Ito, M. (1966). Theoretical plastic stress–strain relationship of a polycrystal and the comparisons with the von Mises and the Tresca plasticity theories. *Int. J. Engng Sci.* **4,** 543–561.

Mindess, S. and Young, J. F. (1981). *Concrete*. Prentice-Hall, NJ.
Nelissen, L. J. M. (1972). Biaxial testing of normal concrete. *HERON* **18,** No. 1, 90 pp.
Oda, M. (1972). Deformation mechanism of sand in triaxial compression tests. *Soils Found.* **12**(4), 1–18.
Oda, M., Nemat-Nasser, S. and Mehrabadi, M. (1982). A statistical study of fabric in a random assembly of spherical granules. *Int. J. Numer. Anal. Meth. Geomech.* **6**(1), 77–94.
Prat, P. C. (1987). Micromechanics modeling and fracture of concrete and geomaterials. Ph.D. Dissertation, Northwestern University, Evanston, IL.
Richart, F. E., Brandtzaeg, A. and Brown, R. L. (1928) A Study of the failure of concrete under combined compressive stress. University of Illinois Engineering Experiment Station Bulletin 189.
Rothenburg, L. and Selvadurai, A. P. S. (1981). Micromechanical definition of the Cauchy stress tensor for particular media. *Mechanics of Structural Media* (Edited by A. P. S. Selvadurai), pp. 469–486. Elsevier, Amsterdam.
Satake, M. and Jenkins, J. T. (1989). *Micromechanics of Granular Materials*. Elsevier, NY.
Shukla, A., Sadd, M. H. and Mei, H. (1990). Experimental and computational modeling of wave propagation in granular materials. *Exp. Mech.* **30,** 377–381.
Taylor, G. I. (1938). Plastic strain in metals. *J. Inst. Metals* **62,** 306–324.
Thornton, C. and Barnes, D. J. (1982). On the mechanics of granular materials. In *IUTAM Conf. on Deformation and Failure of Granular Materials*, Delft, pp. 69–77.